INDERSCIENCE PUBLISHERS
Linking academia, business and industry through research

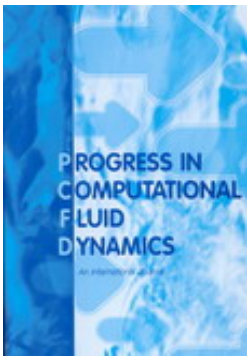


**Progress in Computational Fluid Dynamics, An International Journal**

ISSN online: 1741-5233 - ISSN print: 1468-4349
https://www.inderscience.com/pcfd

# The optimum nozzle exit position and the behaviour of a turbulent flow in an ejector designed for natural draft burner

Chukwunonso F. Nwoye, Chukwunenye A. Okoronkwo, Godswill Nwaji, Humphrey Ogbonnia Okoro, Olisaemeka Nwufo, Emmanuel E. Anyanwu

**DOI:** 10.1504/PCFD.2024.10065410

**Article History:**

| | |
|---|---|
| Received: | 01 July 2023 |
| Last revised: | 11 April 2024 |
| Accepted: | 11 April 2024 |
| Published online: | 06 January 2025 |

# The optimum nozzle exit position and the behaviour of a turbulent flow in an ejector designed for natural draft burner

Chukwunonso F. Nwoye*

Department of Mechanical Engineering,
Akanu Ibiam Federal Polytechnic Unwana Afikpo,
Ebonyi State, Nigeria
Email: royalpriest20@yahoo.com
*Corresponding author

Chukwunenye A. Okoronkwo and Godswill Nwaji

Department of Mechanical Engineering,
Federal University of Technology Owerri, Nigeria
Email: chukwunenyeanthonyokoronkwo@gmail.com
Email: godswillmee@gmail.com

Humphrey Ogbonnia Okoro

Department of Mechanical Engineering,
Akanu Ibiam Federal Polytechnic Unwana Afikpo,
Ebonyi State, Nigeria
Email: okorohumphrey@yahoo.com

Olisaemeka Nwufo and Emmanuel E. Anyanwu

Department of Mechanical Engineering,
Federal University of Technology Owerri, Nigeria
Email: olisaemeka.nwufo@futo.edu.ng
Email: eemmanuelanyanwu@gmail.com

**Abstract:** This study investigated the near and far stream behaviour of a turbulent flow through an ejector at different axial positions of the nozzle. The study was conducted numerically for a throat-to-nozzle exit axial distance of 5 mm–20 mm. The secondary to the primary stream velocity ratio and the magnitude of the boundary layer fluctuation at the nozzle exit increased with the reducing axial distance. The potential core decayed as the flow approached a critical Reynolds number, and the increase in boundary layer fluctuation suppressed the near stream turbulence and momentum transfer by turbulent eddies. The model of the core length as a function of the throat-to-nozzle exit distance revealed a linear profile. Two models described the species concentration along the jet axis as a function of the root mean squared value of the fluctuating velocity because the flow behaved differently near and far streams due to the different controlling mechanisms.

**Keywords:** venturi jet; turbulence; nozzle position; velocity ratio; species mixing; initial conditions.

**Reference** to this paper should be made as follows: Nwoye, C.F., Okoronkwo, C.A., Nwaji, G., Okoro, H.O., Nwufo, O. and Anyanwu, E.E. (2025) 'The optimum nozzle exit position and the behaviour of a turbulent flow in an ejector designed for natural draft burner', *Progress in Computational Fluid Dynamics*, Vol. 25, No. 1, pp.16–30.

**Biographical notes:** Chukwunonso F. Nwoye is a Lecturer at the Department of Mechanical Engineering at Akanu Ibiam Federal Polytechnic Unwana. He has years of experience in teaching and research with interests in turbulence modelling, passive mixing, fluid flow analysis, combustion, and computational fluid dynamics. His publications include 'The investigation of the kinetics of thin-layer drying of fruits using computational fluid dynamics' and 'Changes in the primary nozzle contours and ejector performance'.

Chukwunenye A. Okoronkwo is a Professor of Mechanical Engineering, boasting more than two decades of expertise in teaching and research. His research interests include applied energy studies, robotics, sensors and actuators, material development, computational fluid dynamics, energy policy and planning, and renewable energy. Some of his works include the development of a heuristic algorithm to obtain a control measure to cost function in the manufacturing industry, the transient simulation of hybrid solar collectors and nocturnal radiators in buildings, and the effect of electromagnetic flux density on the ionisation and combustion of fuel.

Godswill Nwaji obtained his PhD in Energy and Power at The Federal University of Technology Owerri, where he currently lectures. He has over ten years of teaching and research experience and has published in several reputable journals. Some of his publications include 'The investigation of kinetics of thin layer drying of fruits using computational fluid dynamics' and 'Hybrid solar water heating and nocturnal radiation cooling system: a review of the progress, prospects, and challenges'. He is interested in energy conversion, material development, diurnal heating, nocturnal cooling, energy policy and planning.

Humphrey Ogbonnia Okoro is a Senior Lecturer at the Department of Mechanical Engineering at Akanu Ibiam Federal Polytechnic Unwana Nigeria. He obtained his PhD in 2024 in Energetic Mechanics at the Federal University of Technology Owerri, Nigeria. His research focus includes Computational fluid dynamics, renewable energy, heat transfer, passive radiative cooling and heating, and its application in buildings. Some of his works include dual-layered titanium oxide-acrylic film on carbon black for passive radiative cooling and thermal performance of diurnal passive radiative systems for space cooling.

Olisaemeka Nwufo has a PhD in Energy and Power and has over a decade of expertise in teaching and research. His research interests include applied energy studies, combustions, computational fluid dynamics, turbulence, energy policy and planning, numerical modelling, and renewable energy. Some of his works include 'The generation of bioelectricity from poultry waste using a microbial fuel cell system' and the 'Investigation of the effect of window glazing on cooling loads of buildings'.

Emmanuel E. Anyanwu is a Professor of Mechanical Engineering, boasting more than three decades of expertise in teaching and research. His research interests include applied energy studies, renewable energy, solar thermal energy engineering, solar refrigeration, computational fluid dynamics, energy policy and planning, and environmental pollution and control. Some of his works include 'Wind characteristics and energy potential for Owerri Nigeria, 'Diesel engine performance of Jatropha Biodiesel', and 'Experimental investigation of passive cooling of buildings using night-time radiant cooling'.

## 1 Introduction

An ejector is a confined jet unit whose geometry is like a venturi (Figure 1). It is also known as the venturi-jet mixer and consists of three sections. The sections include the convergent section, the throat, and the divergent section (the diffuser). The defining geometrical variables of an ejector are the nozzle diameter ($d_N$), the suction tube diameter ($d_S$), the throat diameter ($d_T$), the axial distance between the nozzle exit and the throat ($l_{TN}$), the length of the diffuser ($l_D$), the contraction or convergence angle ($\beta$) and the expansion angle ($\alpha$).

In the ejector flow, the mean flow velocity is increased at the throat while the pressure drops, in line with Bernoulli's principle. The consequent pressure gradient between the throat and the secondary fluid inlet is responsible for pumping the secondary fluid (atmospheric air) into the ejector, and this is the so-called venturi effect. The two streams (fuel jet and the atmospheric air) which flow at different velocities come in contact at the nozzle exit. The consequence of the velocity difference between the layers of the streams in contact is shear stress, which leads to Kelvin-Helmholtz instability. The vortices, which characterise the shear layer, grow in a streamwise direction by pairing and are responsible for air entrainment into the fuel stream. The vortices breakdown into turbulent eddies a short distance from the origin leading to the molecular mixing of the entrained air and the fuel species (Rehab et al., 1997; Liepmann and Gharib, 1992).

Some areas of ejector application include throttling loss recovery in refrigeration systems to improve the refrigeration capacity and reduce compressor power consumption (Guangdi et al., 2023), liquid loading in natural gas extraction (Huizhen et al., 2023), seawater desalination (Jianbo, et al., 2022), and fracturing fluid mixing in oil and gas operations (Long et al., 2020; Yudong, et al., 2021; Dhanesh et al., 2016; Randive et al., 2018). These systems prioritise the secondary fluid pumping and mixing with the primary stream. Other performance indicators include pressure profile, pumping coefficient, the mean velocity at the outlet, axial velocity distribution, and turbulent kinetic energy (Zihzhen et al., 2020; Ali and Mohammed, 2020; Krzysztof and Robert, 2017; Manisha and Bhim, 2017).

Some of the factors that influence performance are the pressure difference between the inlet and outlet section (Yanqi and Wenquan, 2012; Zhang, 2017), the design of the nozzle (Enle et al., 2020; Fatong et al., 2021; Nwoye et al., 2024a), the working fluid (Ali and Mohammed, 2020) and structural parameters of the mixer such as area of throat to nozzle ratio, suction chamber area ratio and nozzle exit position or projection ratio (Agrawal, 2013). Others include the throat contraction ratio, contraction angle, expansion angle, and throat aspect ratio (Yanqi and Wenquan, 2012; Zhang, 2017).

Mass flux correlated positively with the contraction ratio and inlet/outlet pressure differential, but the reverse was the case with diffusion angle (Zhang, 2017). The investigation by Vashahi et al. (2017) showed that contraction ratio affects entrainment the most compared to air inlet diameter and diffuser angle. This position agrees with the investigation by Yanqi and Wenquan (2012) in their study of the effect of structural parameters on hydraulic performance. The performance criteria included the minimum pressure achieved in the unit and the mean velocity at the outlet. Juan et al. (2016) also studied the influence of throat morphology on velocity distribution in ejectors.

The investigators used experiments, computational fluid dynamics (CFD), and analytical models primarily. The CFD investigations comprised the optimisation of the mixing chamber for two throat nozzle ejector (Fatong et al., 2021), the influence of operating conditions on optimum nozzle exit position (Ali and Mohammed, 2020), parametric analysis of inlet pressure and primary nozzle position on performance (William et al., 2020) and optimisation of nozzle structure for maximum gas induction (Enle et al., 2020). Others are parametric investigation by Scott et al. (2008) to identify key features that impact ejector performance and the study of the performance of steam ejectors for use in refrigeration/heat pump systems by Mustafa and Cuneyt (2019). 1D model were developed by Lawn (2002), Hafiz et al. (2020), and Matrio et al. (2021) to investigate the performance of ejectors. Hadi (2017), Schmidt and Hupfer (2021), and Nakagawa et al. (2008) used experiments and CFD simulation. The works by Subramanian et al. (2018) and Voropayev et al. (2011) were solely experimental.

These works, however, placed little or no emphasis on turbulence development and its critical role in system performance. This investigation focused on the changes in the flow structure and turbulence regimes when propane and air are the primary and the secondary streams, respectively, in an ejector designed for natural draft burners at different throat-to-nozzle exit axial distance.

## 2 Materials and methods

Figure 1 and Table 1 show the physical model of the mixer and the geometric parameters, respectively. The throat diameter ($d_T$ = 10 mm) and every other parameter of the mixer except the axial position of the nozzle ($l_{TN}$) were constant. The axial position of the nozzle from the throat increased from 5 mm to 20 mm in the sequence shown in Table 1. The CFD investigation involves the numerical solutions to the incompressible 3D steady-flow Reynolds Averaged Navier Stokes (RANS) and species transport equations for a single-phase flow in the domain. The RANS equation has extra stress terms that include the products of the fluctuating velocities associated with convective momentum transfer due to turbulent eddies called the Reynolds stresses (Versteeg and Malalasekera, 1995; Andrew et al., 2016). Turbulence models are required to predict the Reynolds stresses and close the RANS equation (Salim et al., 2010). Some of these turbulence models used in ejector flow simulation include; the standard $k$-$\varepsilon$ model (Enle et al., 2020; Zihzhen et al., 2020; Zhang, 2017; Yanqi and Wenquan, 2012; renormalisation (*RNG*) $k$-$\varepsilon$ model (Manisha and Bhim, 2017), realisable $k$-$\varepsilon$ model (Vashahi et al., 2017), $k$-$\omega$ SST model (Krzysztof and Robert, 2017) and Reynolds Stress Model (RSM) (Juan et al., 2016). The details of the species transport equation can be found in Nwoye et al. (2024b), Firas et al. (2020), and Versteeg and Malalasekera (1995).

The turbulence models considered in this work were the realisable $k$-$\varepsilon$ model and the RSM. See Versteeg and Malalasekera (1995) and Zagorka et al. (2019) for the details of the equation and their standard constants. They are high Reynolds number turbulence models suitable for core flow, where the inertia forces dominate. The high mean flow velocity gradient in the core flow region or far away from the wall causes instability that produces turbulence. On the other hand, the velocity fluctuation close to the wall is reduced by viscous damping, and the flow behaviour close to the wall is very distinct from that of the core flow. Accurate prediction of the wall-bounded turbulent flow depends on the correct resolution or modelling of the near-wall flow behaviour. Hence, the combination of high Re turbulence models (the realisable $k$-$\varepsilon$ model and the RSM) with the semi-empirical standard wall function for the simulation.

## 3 Mesh generation

The discretisation was by prism layer mesh close to the wall boundary and tetrahedral mesh far away from the wall (Figure 2). In addition to stability in the computation process, it is quicker to generate compared to structured mesh because of the complexity of the geometry. The modelling of the near-wall flow behaviour was by the standard wall function, and the centroid of the first cell adjacent to the wall was scaled to $30 < Y^{+} < 50$ to enable the fitting of the standard wall function in the region (Versteeg and Malalasekera, 1995).

**Figure 1** The diagram of a coaxial ejector (see online version for colours)

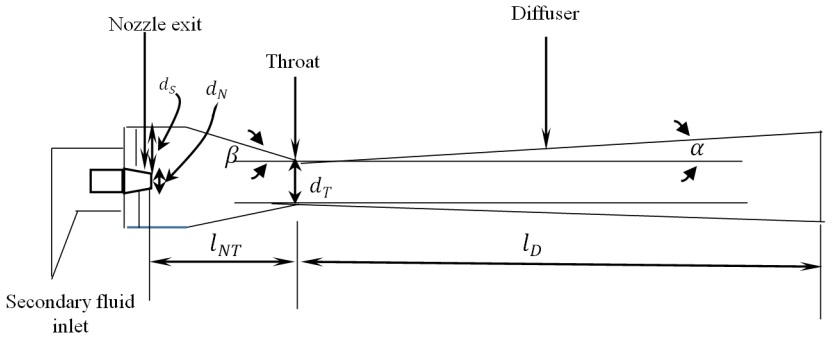


**Figure 2** Mesh outline (see online version for colours)

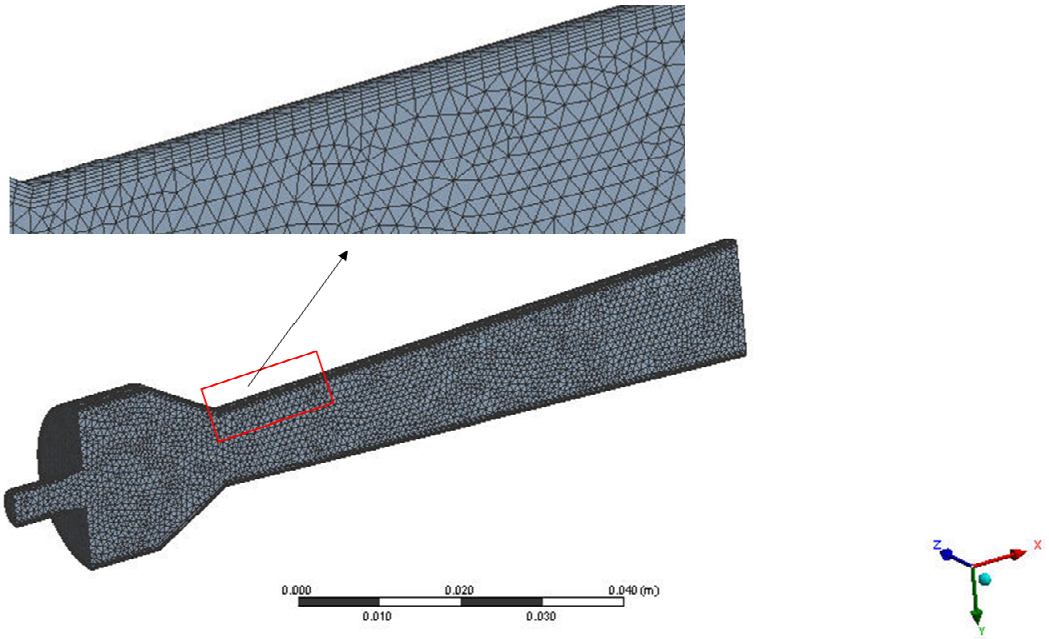


**Figure 3** Variation in (a) velocity, (b) pressure coefficient at the centreline with number of grid elements (see online version for colours)

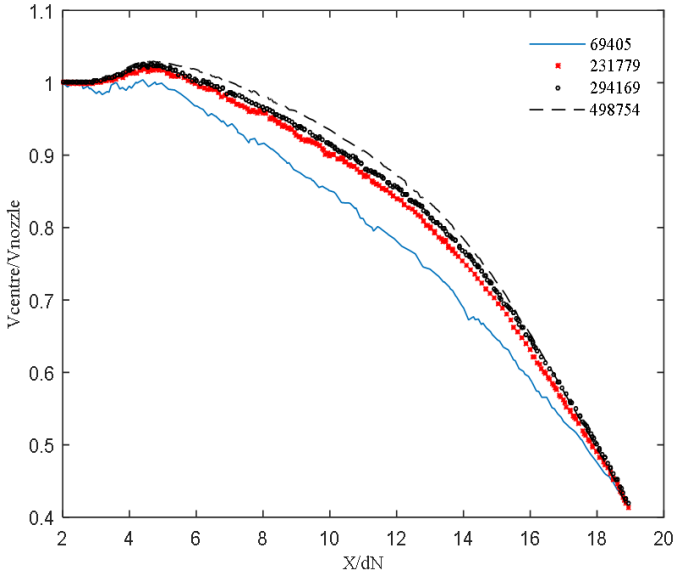


(a)

**Figure 3** Variation in (a) velocity, (b) pressure coefficient at the centreline with number of grid elements (continued) (see online version for colours)

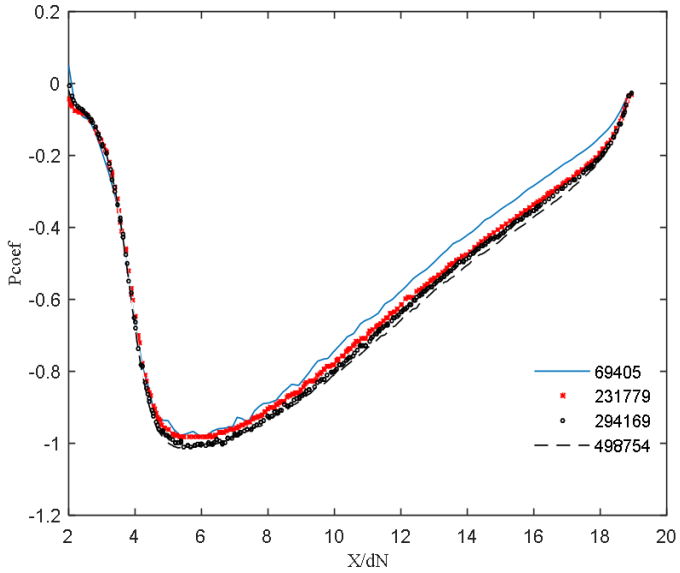


(b)

**Figure 4** Geometry of Binder and Kian experiment

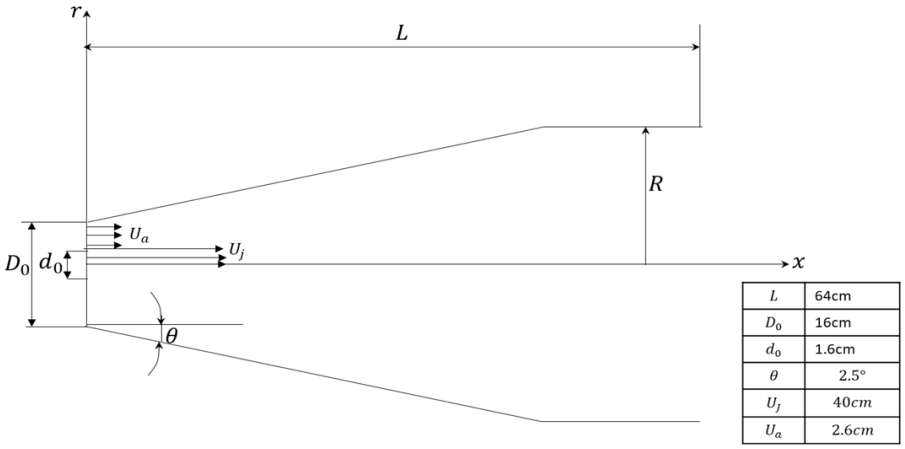


| | |
|---|---|
| $L$ | 64cm |
| $D_0$ | 16cm |
| $d_0$ | 1.6cm |
| $\theta$ | 2.5° |
| $U_j$ | 40$cm$ |
| $U_a$ | 2.6$cm$ |

*Source:* Binder and Kian (1983)

**Figure 5** Centreline velocity decay from models and experiment (see online version for colours)

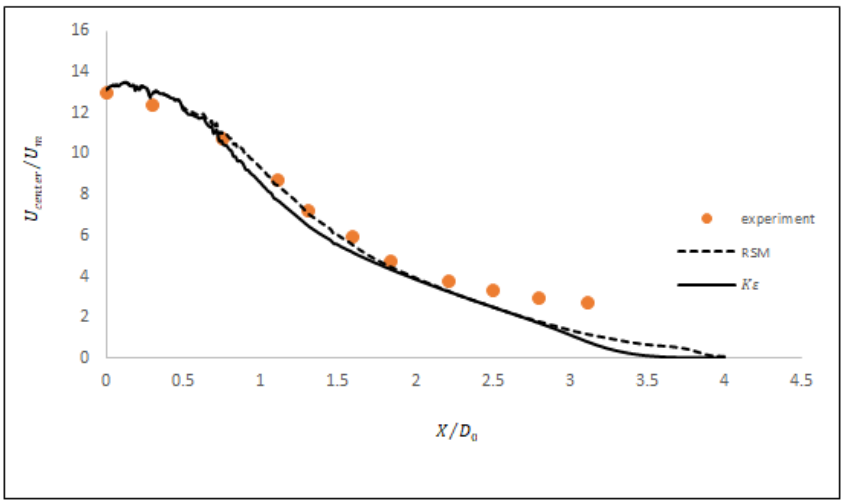

### *3.1 Solution strategy*

The simulation was by ANSYS fluent – a finite volume CFD code. Because of the symmetric nature of the ejector, the computation was carried out in half of the domain to conserve time and computer memory. The model was a pressure-based, steady-state system with propane and air as the motive and secondary fluid, respectively. The properties of fluid were the default in the database. Pressure/velocity coupling was by the coupled algorithm, and spatial discretisation for momentum and turbulent kinetic energy was by second-order upwind. The summary of the boundary conditions is in Table 2. The turbulence viscosity ratio and turbulence intensity at the inlet was 10, and 5%, respectively. The convergence criteria are the globally scaled residual set at $1\times10^{-6}$ for all parameters of interest.

**Table 1** The geometrical parameters of the ejector and their values

| *Parameter* | *Value (mm)* |
|---|---|
| Nozzle diameter ($d_N$) | 5 |
| Suction chamber diameter ($d_S$) | 16 |
| Diffuser length ($l_d$) | 75 |
| Convergence angle ($\beta$) | 30° |
| Divergence angle ($\alpha$) | 2° |
| Nozzle exit position relative to the throat ($l_{TN}$) mm | 5, 10, 15, 20 |
| Throat diameter ($d_T$) mm | 10 |

**Table 2** Boundary conditions used for the simulation

| *Boundary zone* | *Boundary type* | *Value of parameters* | | |
|---|---|---|---|---|
| *Nozzle exit* | *Re* | *2,960* | | |
| | | *Velocity (m/s)* | *Pressure (Pa)* | *Specie mass fraction* |
| Air inlet | Pressure inlet | 0 | 0 | 0.233 ($O_2$) |
| Fuel inlet | Velocity inlet | 2 | - | 1 ($C_3H_8$) |
| Symmetry | axis | - | - | - |
| Outlet | Pressure outlet | - | 0 | - |
| Walls | Wall | No slip | - | - |

## 4 Grid independence study

The proof of the independence of the simulation result on the number of cells was with four grids whose cell count ranged from 69,405 to 498,754. The charts of the pressure coefficient and mean velocity at the centreline for each of the grids are in Figure 3. The mean velocity data [Figure 3(a)], when the cell tally was 69,405, was distinct from the rest. As the cell numbers increased, the disparities became negligible. Also, the variation in pressure coefficient [Figure 3(b)] was more evident in the diffuser. However, the differences became small with the increase in the number of cells. Concerning the mean velocity at the centreline, the highest contrast was at $X/d_N = 10$. When the number of cells increased from 231,779 to 498,754 (a 115.2% increase), the change in centreline velocity and pressure coefficient values, respectively, at $X/d_N = 10$, were 3.2% and 4.3%. 231,779 were an optimal cell counts per accuracy and computation time hence the choice for the computation.

## 5 Model validation

The model was validated using the experiment by Binder and Kian (1983). The geometry, dimensions, and flow conditions at the inlet for the experiment are in Figure 4. The flow conditions are similar to the case under consideration. The velocity decay data from the experiment and simulation using the realisable $k$-$\varepsilon$ model and the RSM showed acceptable agreement in the potential core and the early stages of flow development (Figure 5). The disparities were apparent towards the outlet but more pronounced in the $k$-$\varepsilon$ model. RSM was adjudged superior to the realisable $k$-$\varepsilon$ model and was used for the simulation.

## 6 Results and discussion

The following are the results of the simulation. The Re of the flow based on the diameter of the nozzle and velocity at the nozzle exit was ≈2,960. The result presentation was in terms of the nozzle exit position to the throat diameter ratio $l_{TN}/d_T$.

### *6.1 Velocity analysis*

#### *6.1.1 The radial profile*

Figure 6 shows the radial profile of the mean velocity at the nozzle exit (1 mm from nozzle exit), the throat ($X/d_N = 4$), and the mixer outlet ($X/d_N = 17$). The direct consequence of positioning the nozzle closer to the throat was the steady decrease in the diameter of the secondary fluid inlet $d_s$ (see Figure 1and Figure 9) and the increase in the secondary to the primary stream velocity ratio $V_r$ at the nozzle exit [Figure 6(a)], which affects the potential core length and entrainment (Rehab et al., 1997; Dimotakis, 1991). The approximate $V_r$ values are 0.2, 0.1, 0.08, and 0.07 for $l_{TN}/d_T = 0.5$, 1.0, 1.5 and 2.0, respectively. The streamwise decay of the mean velocity gradient between the streams [Figure 6(b) and Figure 6(c)] also varied even up to the ejector outlet, indicating that the nozzle position did not just affect the near stream flow behaviour but also the far stream momentum transfer by turbulent eddies. Slessor et al. (1998) revealed that even small changes in the inflow or boundary layer condition can influence the large-scale structure, shear-layer growth rate, molecular mixing, and chemical product formation.

**Figure 6** Radial velocity profile at (a) nozzle exit, (b) $X/d_N = 4$, (c) $X/d_N = 17$ (see online version for colours)

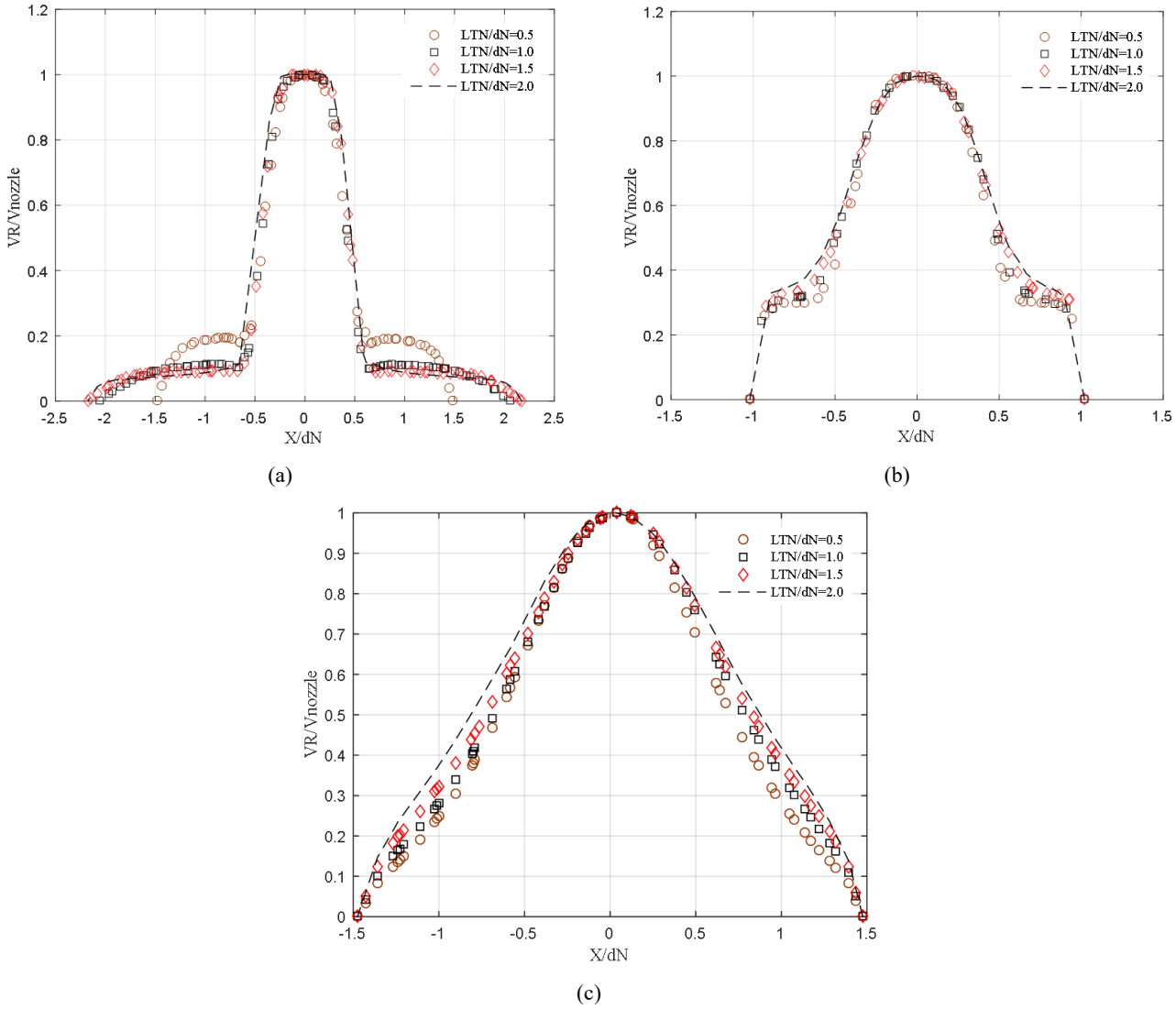


**Figure 7** Centreline velocity profile (see online version for colours)

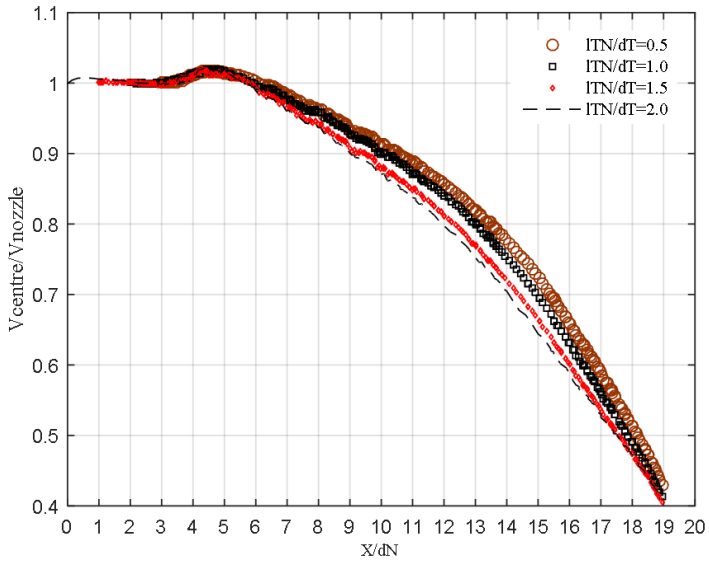

**Figure 8** Dependence of the potential core length on the nozzle exit position (see online version for colours)

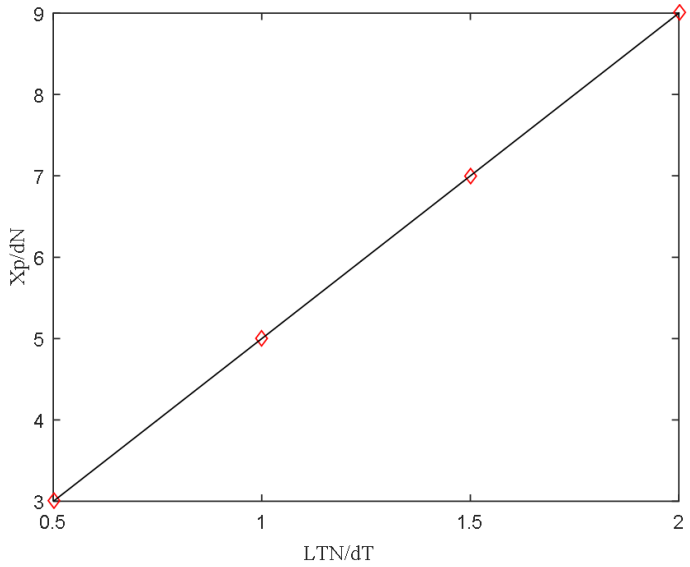


**Figure 9** Velocity contours at each nozzle position (see online version for colours)

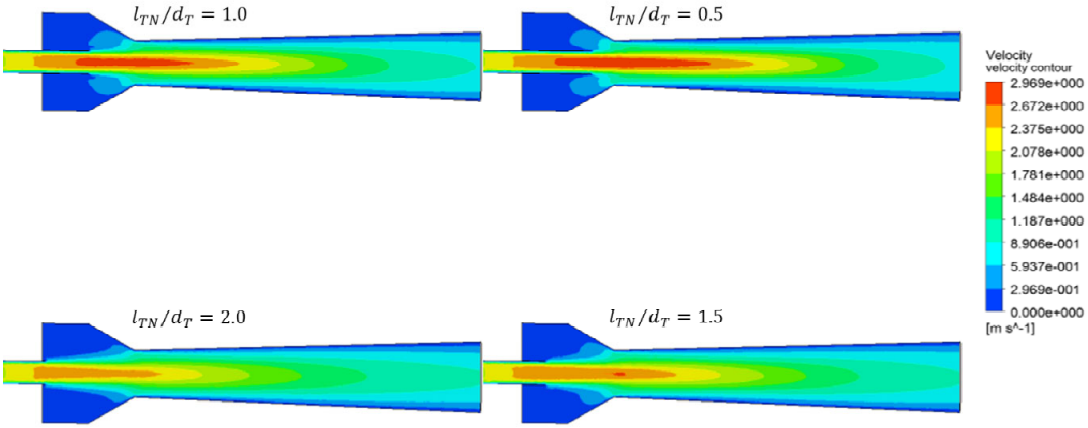


### *6.1.2 The potential core length*

The centreline velocity decay curve (Figure 7) showed the potential core (horizontal portion) and the turbulent portion characterised by rapid decay. In the range of this study ($0.5 \leq l_{TN}/d_T \leq 2.0$), the potential core length increased in equal proportion with the axial distance between the nozzle exit and the throat. This is logical, considering that the flow velocity increases close to the throat (Figure 7) and the Reynolds number approaches a critical value which is part of the conditions for the flow transition to full scale turbulence (Slessor et al., 1998). The potential core length is also affected by the velocity difference between the two streams. From the model developed by Dimotakis (1991) to relate the shearlayer spread with density ratio and velocity ratio, a decrease in the velocity difference or an increase in $V_r$ will reduce the shear layer spread and entrainment, which, from the works of Liepmann and Gharib (1992), relates to the potential core length. Rehab et al. (1997) derived an inverse relationship between the outer-to-inner stream velocity ratio and the potential core length. They also expressed the potential core length as a function of entrainment velocity.

In Figure 7, for the throat-to-the-nozzle exit distance in the range $0.5 \leq l_{TN}/d_T \leq 2.0$, the mean velocity at the ejector axis remained relatively unchanged from the origin to $X/d_N = 3$ and increased to ≈1.03 $V_{nozzle}$ at $X/d_N = 4.5$ before the start of the decay process. This axial distance between the nozzle exit and $X/d_N = 4.5$ is the potential core length ($X_p$). Based on this estimate, $X_p$ varied with the nozzle position, as shown Table 3. Equation (1) relates $X_p$ with the axial position of the nozzle $l_{TN}/d_T$ (Figure 8).

$$\frac{X_p}{d_N} = 4\frac{l_{TN}}{d_T} + 1 \tag{1}$$

**Table 3** $l_{TN}/d_T$ ratio and the corresponding potential core length

| Potential core length ($X_p$) | 1.5 | 2.5 | 3.5 | 4.5 |
|---|---|---|---|---|
| $l_{TN}/d_T$ | 0.5 | 1 | 1.5 | 2 |

Kabashi (2020) estimated the $X_p$ as $3d_N$ when the exit velocity was 1.39 ms$^{-1}$ and 2.34 ms$^{-1}$ and $5d_N$ when the velocity was up to 3.89 ms$^{-1}$. Syed et al. (2019) also showed $X_p$ extending to $7d_N$ in free jets and $2d_N$ in plunging jets.

### 6.1.3 The centreline velocity decay

The conditions for the breakdown of the streamwise vortices to turbulent eddies and transition to full-scale turbulence were satisfied at $X/d_N$ = 4.5 for all nozzle positions. One of such conditions was an appropriately large Re and stems from the need for the inertial forces to dominate the viscous forces and also to develop and sustain a sufficiently large range of scales and small-scale eddies, which randomly orients the vectors of the physical quantities that characterised the flow in all spatial (3D) directions, and allow for the specie mixing which is of interest in combustion systems (Slessor et al., 1998; Zagorka et al., 2019). The local Reynolds number based on the jet half-width and the velocity difference between the primary and the secondary streams at $X/d_N \approx 4.5$ was ≈1,000. Revill (1997) considered a jet fully turbulent for Re in the range 1,000 < Re < 2,000. See also Versteeg and Malalasekera (1995) for additional discussion. Another documented requirement for good mixing is a minimum downstream distance from the origin or the number of large-scale interactions. This implies that for a constant length of the mixing tube, we expect a state of improved mixing if the axial distance between the throat and the nozzle exit is longer. The instantaneous picture of the near field flow structure by Rehab et al. (1997) showed a more dispersed structure at the transition point at a longer potential core length. This suggests a higher proportion of small-scale eddies at the turbulence transition point and better downstream mixing prospects.

The initial condition of the nozzle exit boundary layer (the magnitude of fluctuation) will profoundly affect the shear-layer growth rate. A turbulent boundary layer at the nozzle exit will slow down the growth rate of a coaxial or axisymmetric jet. This position agrees with the experiment by Parker et al. (2001), which revealed that the nozzle exit boundary perturbation with a trip ring will suppress downstream turbulence and the shear layer growth rate [see Slessor et al. (1998) for additional discussion and references]. The velocity contour in Figure 9 revealed an increase in the mean velocity changes at the nozzle exit when the nozzle was closer to the throat. This, as expected, increased the boundary layer turbulence (Figure 11). The effect was a suppression of the near-stream turbulence and far-stream momentum transfer by turbulent eddies and explains the variations in the streamwise decay of the mean velocity observed in Figure 6 and Figure 7.

### 6.1.4 Dynamic self-similarity

The flow pattern became similar after $6d_N$ (shortly after the turbulence transition). This is the self-preserving or the self-similarity state (Sandip and Michael, 1997). The profile in Figure 10 showed the flow pattern at $7 \le X/d_N \le 17$ for $l_{TN}/d_T$ = 1. The curves were independent of the axial distance X and modelled by equation (2), which is a function of the ratio of the radial distance to the mixing layer width($\aleph = R/\delta$).

$$\frac{V_R}{V_{\max(x)}} = 0.11\aleph^3 - 0.37\aleph^2 - 0.24\aleph + 1 \quad (2)$$

where $V_R$ is the velocity at radial position R, standardised by the maximum velocity at the axial point of interest $V_{\max(x)}$. In the investigation by Cafiero and Vassilicos (2019), the self-similar state of the mean velocity started from $X/d_N$ = 6 up to $X/d_N$ = 54, the furthest streamwise distance of their measurement.

**Figure 10** The dynamic self-similarity of the flow (see online version for colours)

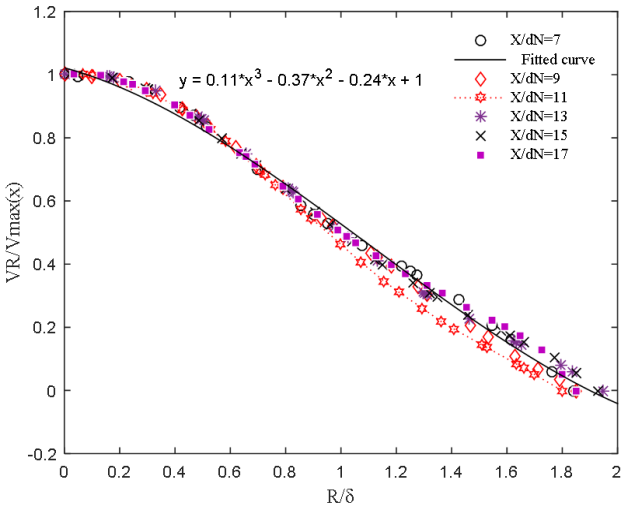


## 6.2 Turbulence analysis

### 6.2.1 Turbulence at the nozzle exit

Turbulence estimation was by the root-mean-square (r.m.s) value of the fluctuating velocity components ($u'$, $v'$, and $w'$). The components $u'$, $v'$, and $w'$ are the velocities in the $x$, $y$, and $z$ planes, respectively, with the mean velocity subtracted out, and they measure the average magnitude of the velocity fluctuations. Figure 11 shows the profile of the magnitude of velocity fluctuations $u'$ standardised by the maximum mean velocity ($V_{\max(x)}$) at the nozzle exit for each nozzle position. This was similar to the profile obtained by Rehab et al. (1997) in their experimental study of flow regimes in coaxial jets. The level of fluctuations was the same in the jet axis (≈0.03 $V_{\max(x)}$), the secondary stream axis (≈0), and the mixing layer (≈0.08 $V_{\max(x)}$), irrespective of the nozzle position. The fluctuations in the boundary layer were highest (≈0.06 $V_{\max(x)}$) when the nozzle was 5 mm ($l_{TN}/d_T$ = 0.5) away from the throat. This disparity in the boundary layer fluctuation at the nozzles' trailing edge partly affects the growth rate of the mixing layer. Other factors affecting the mixing layer growth are the velocity and density ratios of the streams (Alexander and James, 2012; Strykowski and Niccum, 1992).

**Figure 11** The radial profile of the r.m.s values of velocity fluctuation ($u'$) at the nozzle exit (see online version for colours)

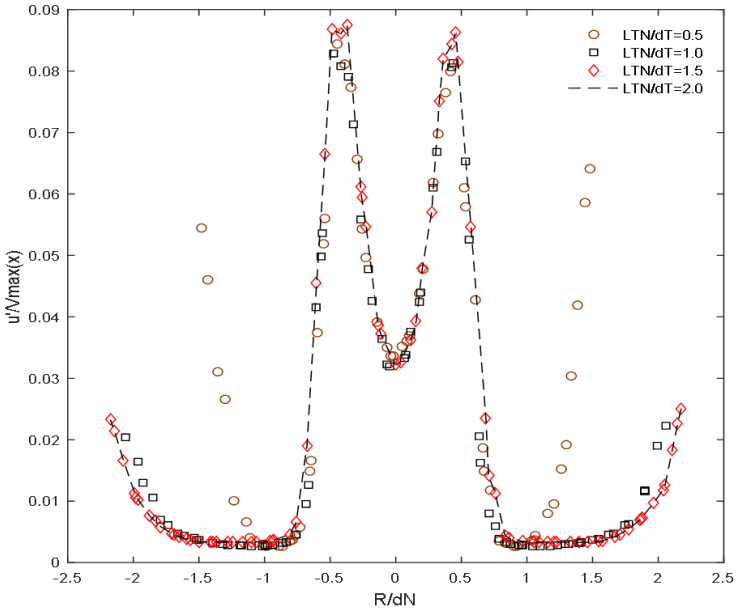


**Figure 12** The mean velocity profile ($V_R$) and the r.m.s velocity fluctuation ($V_i'$) at (a) $X/d_N = 4$, (b) $X/d_N = 17$ (see online version for colours)

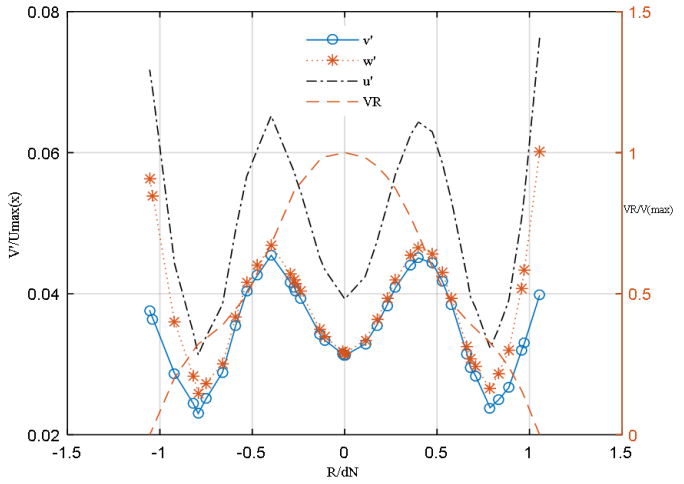


(a)

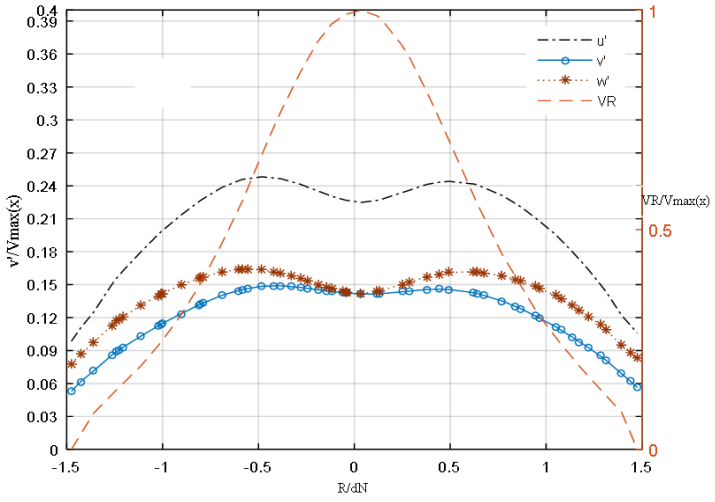


(b)

### 6.2.2 Downstream evolution of turbulence

Figure 12 shows the radial profile of the mean velocity ($V_R$) and the r.m.s data of the fluctuating velocity components at $X/d_N = 4$ and $X/d_N = 17$, respectively, for $l_{TN}/d_T = 2.0$. There was an overall increase in the fluctuation level downstream. For example, in the jet axis, the $u'$ increased from ≈0.03 $V_{max(x)}$ at the nozzle exit (see Figure 11) to ≈0.04 $V_{max(x)}$ at the throat [Figure 12(a)]. The boundary layer fluctuation also increased to ≈0.07 $V_{max(x)}$ from ≈0.025 $V_{max(x)}$.

Overall, the flow fluctuated more in the shear layers (between the streams and adjacent to the wall) due to the velocity gradients that causes shear and instability growth that leads to turbulence. There is no turbulence production in the jet axis. The recorded fluctuations were due to turbulence transport by eddies across the centreline from the adjacent shear layers, hence the relatively low fluctuation (Versteeg and Malalasekera, 1995). The $u'$ fluctuated the most of the three normal stresses (Figure 12), which highlights the anisotropic nature of the turbulence. At the outlet [Figure 12(b)], the magnitude of the fluctuations in the mixing layer had increased to ≈0.24 $V_{nozzle}$, but with a more gentle gradient due to the decay of the momentum difference between the two streams as they interact. There was also the boundary layer fluctuations suppression far stream due to viscous damping. The implication of the gentle incline was the waning of the turbulence production rate observed from $X/d_N = 16$ in Figure 13.

### 6.2.3 Turbulence at the jet axis

Figure 13 shows the magnitude of fluctuation at the jet axis for each nozzle position. It appears that the downstream turbulence developed in three stages. First ($0 < X/d_N < 3.5$), the fluctuation was steady because of the dominance of streamwise vortices. The length of this regime for each nozzle position was proportional to the corresponding core length (see Figure 7). Next, ($4 < X/d_N < 16$), the fluctuation increases due to the breakdown of the vortices into turbulent eddies with a wide range of scales. The intersection of these two regimes marked the point of turbulence transition in the flow. In the third stage, the velocity fluctuation curve flattened because of the attenuation of the shear that produced the turbulence.

### 6.2.4 Self-similarity of turbulence

The $u'$ profile at $X/d_N = 4$ and $X/d_N = 17$ for each nozzle position is in Figure 14. The effect of the initial condition diminished downstream of the flow. For example, the percentage difference between the peak values of the magnitude of velocity fluctuation at the throat when the nozzle was at $l_{TN}/d_T = 2.0$ and when it was $l_{TN}/d_T = 0.5$ was ≈25%. This value reduced to ≈7% at the outlet and even more for $l_{TN}/d_T = 0.5$, 1.0, and 1.5, where the disparities at the outlet were negligible. It follows that just as with dynamic self-similarity (Figure 10), turbulence structure also reaches a self-similar state at a greater distance from the origin (Versteeg and Malalasekera (1995; Gauding et al., 2021). The self-similarity behaviour of turbulence structure began at $X/d_N = 14$ in the investigation by Cafiero and Vassilicos (2019). This self-similarity behaviour is due to the diminishing effect of the initial condition and requires a minimum downstream distance to achieve (Slessor et al., 1998).

**Figure 13** Magnitude of the velocity fluctuation ($u'$) at the centreline (see online version for colours)

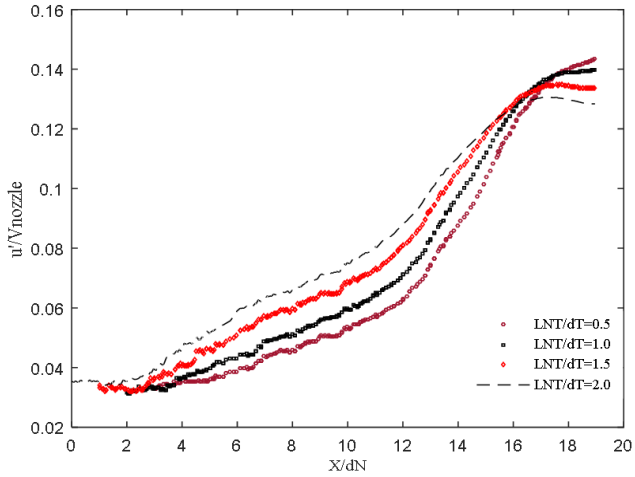


**Figure 14** The Magnitude of velocity fluctuation at (a) $X/d_N = 4$, (b) $X/d_N = 17$ for each nozzle position (see online version for colours)

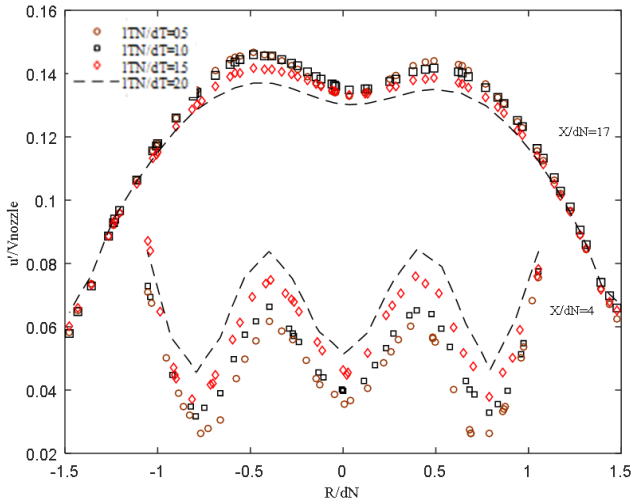


### 6.3 Pressure analysis

Figure 15 is the pressure coefficient plot at the centreline for each nozzle position. The pressure decreased to a minimum at $X/d_N \approx 5$ and increased gradually in the diffuser because of the decrease in flow velocity. The pressure difference between the throat and the nozzle exit and the pressure recovery rate in the diffuser increased with the $l_{TN}/d_T$ ratio. However, the minimum pressure value and the point where it occurred were independent nozzle positions.

**Figure 15** Centreline pressure profile at different nozzle position (see online version for colours)

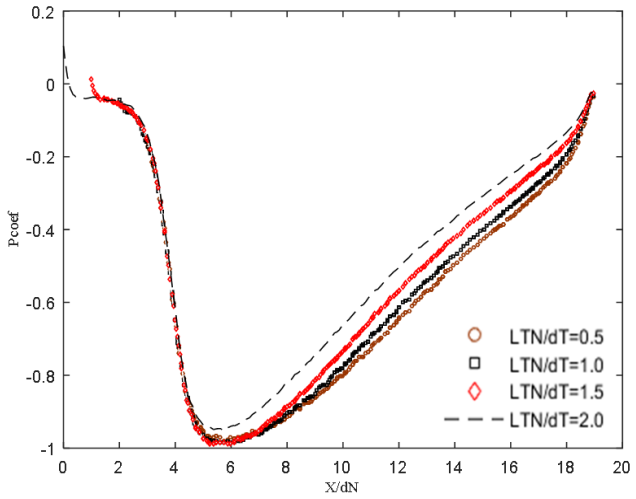


**Figure 16** The $ma_f$ profile at the jet axis (see online version for colours)

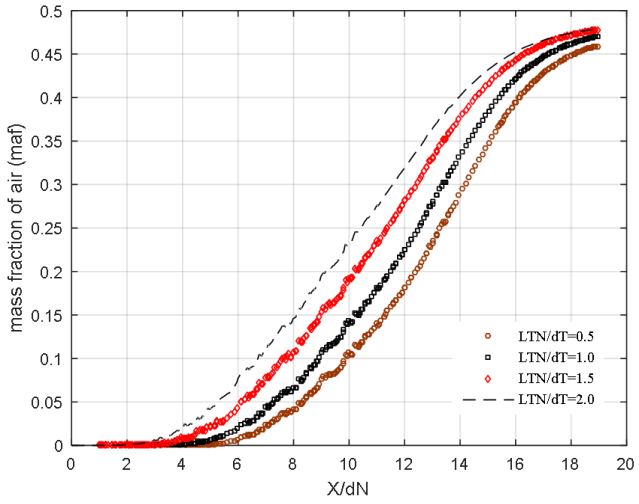


**Figure 17** Radial distribution of $ma_f$ at $X/d_N = 4$ and $X/d_N = 17$ (see online version for colours)

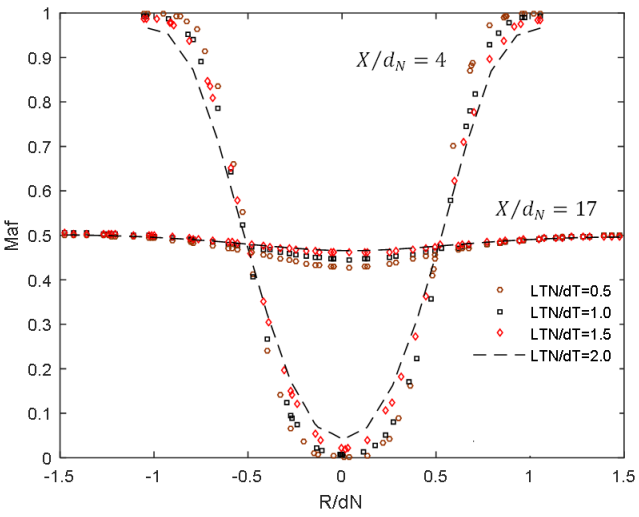


## *6.4 Entrainment and mixing performance*

The entrainment and the mixing performance were analysed using the mass fraction of air at the centreline and its radial distribution at the throat and ejector outlet, respectively. Figure 16, which has a similar profile to the experimental measurement by Villermaux and Rehab (2000), shows the average concentration profile of air along the jet axis. The flow evolved from the initial specie segregation ($ma_f = 0$) at the nozzle exit to a state of a near uniform mixture ($0.45 < ma_f < 0.48$) at the outlet. The profile revealed three different regimes of the air species concentration increase in the jet axis. The first regime spanned $3d_N$ for all nozzle positions and had a gentle incline, attributed to molecular diffusion. The second one, which occurred after a transition period, was steep due to the formation of turbulent eddies. The third showed the fully-mixed regime characterised by a gradual flattening of the curve as the system turbulence approaches a steady state (Rehab et al., 1997; Syed, et al., 2019). The entrainment and mixing process resulted from the initial instability in the interfacial area of the two streams through the mechanism described by Liepmann and Gharib (1992). The near field flow structure experiment by Kabashi (2020) revealed a reversal of the gentle and steep incline that characterised the first and second regimes, respectively, when the Re based on the nozzle exit diameter increased to 7,600 < Re < 9,300 from ≈3,000. Also, the length of the first regime reduced to $2d_N$, from $3d_N$ at 7,600 < Re < 9,300. The investigation was between $0 < X/d_N < 14$ and did not capture the fully-mixed regime observed from ≈16 $X/d_N$ in Figure 16.

Figure 17 shows the concentration profile of air at the throat and the ejector outlet. At the throat was a gradual onset of molecular diffusion and a profile spread that scaled with the distance from the nozzle exit.

**Figure 18** The fluctuation magnitude and $ma_f$ data at centreline for $l_{TN}/d_T = 1$ (see online version for colours)

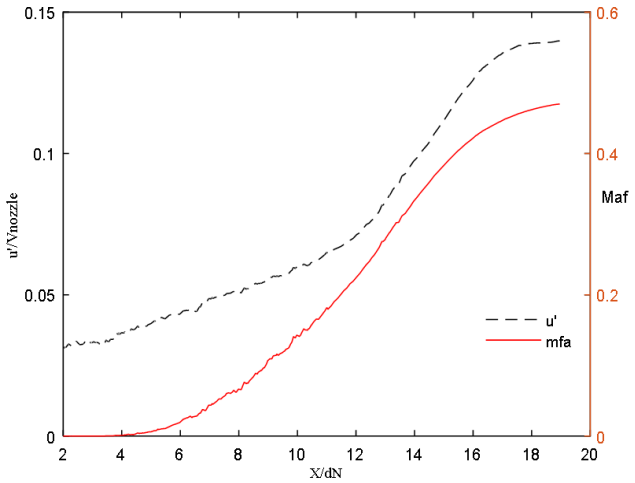


The change of species concentration along the axis was due to mass and momentum exchange across the centreline by the turbulent eddies. Thus, increasing the system's turbulence will facilitate mixing and concentration change. Figure 18 shows a strong correlation between the

fluctuation magnitude and air concentration at the centreline. We predict the centreline concentration as a function of the fluctuation magnitude with two sets of quadratic equations (Figure 19). The first [equation (3)] accounted for the transition regime, while the second [equation (4)] modelled concentration growth in the turbulent and the fully-mixed region

$$ma_f = 213.9u'^2 - 14.69u' - 0.2471 \quad (3)$$

$$ma_f = 21.73u'^2 + 8.12u' - 0.2502 \quad (4)$$

**Figure 19** The plot $ma_f$ as a function of r.m.s velocity fluctuation $u'$ (see online version for colours)

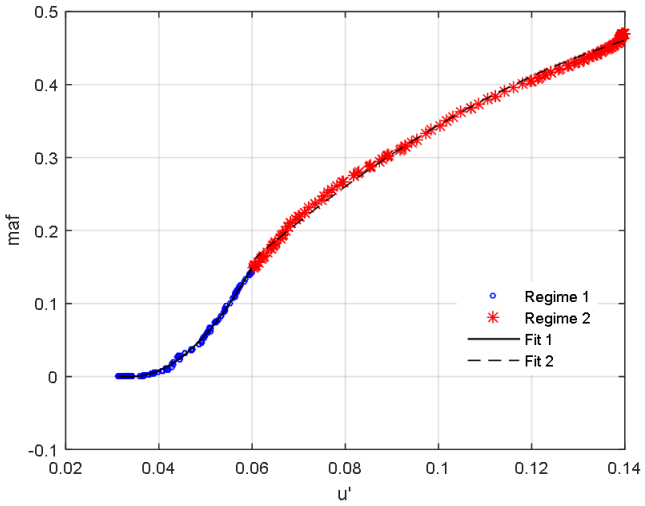


## 7 Conclusions

This study investigated the turbulent flow structure in an ejector designed for a natural draft burner at different throat-to-nozzle exit axial distances. Positioning the nozzle closer to the throat increased the secondary to the primary stream velocity ratio ($V_r$) and the magnitude of the boundary layer fluctuations, which profoundly affected the near and the far stream flow behaviour.

Rehab et al. (1997) described the secondary to the primary stream interaction process at different $V_r$. The $V_r$ had an inverse relationship with the potential core length and the entrainment (Dimotakis, 1991; Liepmann and Gharib, 1992). Similarly, the increase in boundary layer fluctuations suppressed the near stream turbulence and the shear layer growth rate.

Different mechanisms controlled the near and far stream behaviour of the flow. The near-stream turbulence structure revealed a transition regime dominated by streamwise vortices (Rehab et al., 1997). The fully turbulent regime, characterised by rapid mixing, followed afterward, after the breakdown of the vortices into turbulent eddies with a wide range of scales. The steady-state regime occurred towards the end of the mixing tube following the decay of the momentum differences between the streams and the consequent attenuation of the shear that produced the turbulence.

The change in air concentration along the jet axis increased in proportion to the turbulence. Two models captured the air concentration change as a function of the r.m.s value of the centreline velocity fluctuation. The first accounted for the flow behaviour from the origin to the end of the transition, while the second captured the rapid mixing and the steady state regimes.

## Acknowledgements

This work received sponsorship from TETFUND (*TETFUND/ES/AST&D*).

## References

Agrawal, K.S. (2013) 'Performance of venturi scrubber', *International Journal of Engineering Research and Development*, Vol. VII, No. 11, pp.53–69.

Alexander, S.S. and James, D. (2012) 'Mixing properties of coaxial jets with large velocity ratios and large inverse density ratios', *Physics of Fluid*, Vol. XXIV, No. 2012, DOI: 10.1063/1.4711396.

Ali, H. and Mohammed, B. (2020) 'CFD analysis of operating condition effects on optimum nozzle exit position of a supersonic ejector using the refrigerant R134a', *Comptes Rendus Mécanique*, pp.1–14, DOI: 10.5802/crmeca.60.

Andrew, P.L., Martin, S. and Siow, Y.L. (2016) 'Modelling high Re flow around a 2D cylindrical bluff body using the k-w (SST) turbulence model', *Progress in Computational Fluid Dynamics*, Vol. XVI, No. 1, pp.48–57.

Binder, G. and Kian, K. (1983) 'Confined jets in a diverging nozzle', *Turbulent Shear Flow*, Karlsruhe, Vol. 4, pp.18–23.

Cafiero, G. and Vassilicos, J.C. (2019) *Non-Equilibrium Turbulence Scaling and Self-Similarity in Turbulent Planar Jet*, Proceedings A, Royal Society Publishing, pp.1–25, DOI: 10.1098/rpsa.209.0038.

Dhanesh, P., Ashvinkumar, C., Arto, L., Matti, H., Jari, H. and Kishorilal, A. (2016) 'Numerical simulation of bubble coalescence and break-up in multinozzle jet ejector', *Journal of Applied Mathematics*, pp.1–19, DOI: 10.1155/2016/|5238737.

Dimotakis, P.E. (1991) *Turbulent Free Shear Layer Mixing and Combustion*, Graduate Aeronautical Laboratories California Institute of Technology, California.

Enle, X., Xiaofeng, J. and Long, D. (2020) 'Optimizing conical nozzle of venturi ejector in ejector loop reactor using computational fluid dynamics', *Korean J. Chem. Eng.*, Vol. XXXVII, No. 11, pp.1829–1835, DOI: 10.1007/sl1814-020-0607-1.

Fatong, J., Dazhang, Y. and Jing, X. (2021) 'Numerical investigation on the performance of two-throat nozzle ejectors with different mixing chamber structural parameters', *Energies*, Vol. XIV, No. 6900, pp.1–16, DOI: 10.3390/en14216900.

Firas, D., Stefan, P. and Schneiderbauer, S. (2020) 'On fast modeling of species transport in fluidized beds using recurrence computational fluid dynamics', *Particle Technology and Fluidization*, pp.1–20, DOI: 10.1002/aic.16931.

Gauding, M., Bode, M., Brahami, Y., Varea, E. and Danaila, L. (2021) 'Self-similarity of turbulence jet flows with internal and external intermittency', *J. Fluid. Mech.*, Vol. CMIXX, No. 41, pp.1–35, DOI: 10.1017/jfm.2021.399.

Guangdi, L., Hongxia, Z., Jianqiang, D., Lei, W. and Heng, Z. (2023) 'Performance improvement of CO2 two-phased ejector by combining CFD modelling, artificial neural network and genetic algorithm', *International Journal of Refrigeration*, Vol. CLIV, No. 2023, pp.151–167.

Hadi, R. (2017) *Investigation of Radial flow Ejector Performance through Experiment and Computational Simulation*, University of Southern Queens Land Australia, Southern Queens Land.

Hafiz, A.M., Hafiz, M.A., Zabdur, R., Beomjoon, L., Young-Jin, B., Jongjae, C. and Muhammad, S.B. (2020) 'Numerical modeling of ejector and development of improved methods for design of ejector-assisted refrigeration system', *Energies*, Vol. XIII, No. 5835, pp.1–19.

Huizhen, L., Chengzhen, L., Jian, M., Lin, M. and Xiukun, J. (2023) 'Study on improving liquid carrying performance of annular jet pump gas well with static mixer', *SCI*, Vol. XII, No. 2024, pp.70–86, DOI: 10.1002/ese3.1617.

Jianbo, R., Heli, Z., Min, W., Chao, M., Yingzhen, W. and Quiang, L. (2022) 'Design and investigation of a dynamic auto-adjusting ejector for the MED-TVC desalination system driven by solar energy', *Entropy*, Vol. XXIV, No. 1815, pp.1–15, DOI: 10.3390/e24121815.

Juan, M., Carmen, P.V., Benito, D.A., Guilherme, D.B. and Denise, V.V. (2016) 'Geometry and head loss in venturi injectors through computational fluid dynamics', *Journal of the Brazilian Association of Agricultural Engineering*, Vol. XXXVI, No. 3, pp.482–491, DOI: 10.1590/1809-4430.

Kabashi, A. (2020) 'Near-field flow structure and entrainment of a round jet at low exit velocities: implications on microclimate ventilation', *Computation*, Vol. VIII, No. 100, pp.1–15, MDPI, DOI: 10.3390/computation8040100.

Krzysztof, S. and Robert, G. (2017) 'The mixing hydrodynamics and efficiency of the venturi jet mixer', *Technical Transaction*, Vol. XI, pp.95–106.

Lawn, C.J. (2002) 'A simple method for design of gas burners ejectors', *Journal of Mechanical Science*, Vol. CCXVII, pp.1–31.

Liepmann, D. and Gharib, M. (1992) 'The role of streamwise vorticity in near-field entrainment of round jets', *Journal of Fluid Mechanics*, Vol. CCXLV, pp.643–668, Doi.org /10.1017/S0022112092000612.

Long, F., Zengliang, L., Mingchao, D., Zhaocheng, S. and Chunyong, F. (2020) 'Computational fluid dynamics analysis and design optimisation of a porous annular powder-liquid mixer', *Energy Science and Engineering*, Vol. 8, No. 2020, pp.1149–1164, DOI: 10.1002/ese3.575.

Manisha, B. and Bhim, C.M. (2017) 'Prediction of hydro dynamic characteristics of a venturi scrubber by using CFD simulation', *South African Journal of Chemical Engineering*, Vol. XXIV, No. 2017, pp.222–231.

Matrio, P., Florian, W., Christian, J., Stefan, P., Bernhard, S., Franz, W. and Michael, H. (2021) 'Design and simulation of gas burner ejectors', *Carbon Resources Conversion*, Vol. IV, No. 2021, pp.28–35.

Mustafa, A. and Cuneyt, E. (2019) *Three Dimensional CFD Modeling of a Steam Ejector*, Taylor & Francis Group, pp.1–12, DOI: 10.1080/15567036.2019.1649326.

Nakagawa, M., Berana, M.S. and Harada, A. (2008) 'Shock waves in supersonic two-phase flow of CO2 in converging-diverging nozzles', *International Refrigeration and Air Conditioning Conference*, Purdue e-Pubs, Purdue, pp.1–7.

Nwoye, C.F., Okoro, H., Okoronkwo, C., Nwaji, G., Nwufo, O. and Anyanwu, E. (2024a) 'Changes in primary nozzle contours and ejector performance – a numerical study', *Int. J. Adv. Sci. Eng.*, Vol. X, No. 2024, pp.3495–3507, https://doi.org/10.29294/IJASE.10.3.2024.3495-3507

Nwoye, C.F., Okoronkwo, C. and Ezenwa, O.N. (2024b) 'Investigation of the kinetics of thin layer drying of fruits using computational fluid dynamics', *Progress in Computational Fluid Dynamics*, Vol. XXIV, No. 1, pp.54–64.

Parker, R., Rajagopalan, S. and Antonia, R.A. (2001) 'Control of axisymmetric jet using passive ring', *14th Australasian Fluid Mechanics Conference*, Adelaide University, Adelaide, pp.769–722.

Randive, P., Singh, D., Varghese, V. and Barde, A. (2018) 'Study of jet mixing in flocculation process', *IJIRMPS*, Vol. VI, No. 4, pp.76–84.

Rehab, H., Villermaux, E. and Hopfinger, E.J. (1997) 'Flow regimes of large-velocity-ratio coaxial jets', *J. Fluid Mech.*, Vol. 345, No. 1997, pp.357–381.

Revill, B.K. (1997) *Mixing in the Process Industries*, Elsevier, DOI: 10.1016/B978-0-7506-3760-2.X5020-3.

Salim, S.M., Ariff, M. and Cheah, S.C. (2010) 'Wall y+ approach for dealing with turbulent flows over a wall bounded cube', *Progress in Computational Fluid Dynamics*, Vol. X, Nos. 5/6, pp.341–351.

Sandip, G. and Michael, R.M. (1997) 'A numerical study of self-similarity in a turbulent plane wake', *Phys. Fluids*, Vol. IX, No. 6, pp.1729–1739.

Schmidt, R. and Hupfer, A. (2021) 'Design and numerical simulation of ejector nozzles for very small turbojet engines', *CEAS Aeronautical Journal*, Vol. XII, No. 2021, pp.923–940, DOI: 10.1007/s13272-0121-00537-3.

Scott, D., Aidoun, Z., Bellache, O. and Ouzzane, M. (2008) 'CFD simulation of a supersonic ejector for use in refrigeration application', *International Refrigeration and Ir Condition Conference*, Purdue, pp.1–8.

Slessor, M.D., Bond, C.L. and Dimotakis, P.E. (1998) 'Turbulent shear-layer mixing at high reynolds numbers: effects of inflow conditions', *J. Fluid Mech.*, Vol. CCCLXXVI, pp.115–138.

Strykowski, P.J. and Niccum, D.L. (1992) 'The influence of velocity and density ratio on the dynamics of spatially developing layers', *Physics of Fluid*, pp.770–781, DOI: 10.1063/1.858294.

Subramanian, H.G., Nagarjun, S., Kumar, S.K., Kumar, A.B., Srikanth, V. and Srikrishnan, A.R. (2018) 'Mixing enhancement using Chevron nozzle studies on free jets and confined jets', *Sadhana*, Vol. XLIII, No. 109, DOI: 10.1007/s1204-018-0898-7.

Syed, H.H., Tianqi, G. and Pavlos, V.P. (2019) 'Flow field evolution and entrainment in a free surface plunging jet', *Physical Review Fluids*, Vol. IV, No. 104603, pp.1–22, DOI: 10.1103/PhysRrvFluids.4.10460

Vashahi, F., Ra, S., Choi, Y. and Lee, J.K. (2017) 'Influence of design parameters on the air/liquid ratio of an air induction nozzle', *Journal of Mechanics*, DOI: 10.1017/jmech.2017.12.

Versteeg, H.K. and Malalasekera, W. (1995) *An introduction to Computational Fluid Dynamics an Introduction*, Longman Scientific and Technical, New York.

Villermaux, E. and Rehab, H. (2000) 'Mixing in coaxial jet', *J. Fluid. Mech*., Vol. CDXXV, No. 2000, pp.161–185.

Voropayev, S.I., Sanchez, X., Nath, C., Webb, S. and Fernando, H.J. (2011) 'Evolution of confined turbulent jet in a long cylindrical cavity: homogenous fluid', *Physics of Fluid*, Vol. XXIII, No. 115106, pp.1–11.

William, O.M., José, A.P., Iván, D.P., Johan, S.Z. and John, A.H. (2020) 'Analysis of a jet pump performance under different primary nozzle positions and inlet pressures using two approaches: one dimensional analytical model and three dimensional CFD simulations', *Journal of Applied and Computational Mechanics*, Vol. VI, No. 2020, pp.1228–1244.

Yanqi, S. and Wenquan, N. (2012) 'Simulating the effects of structural parameters on the hydraulic performances of VenturiTube', *Modelling and Simulation in Engineering*, Vol. MMXII, pp.1–7, DOI: 10.1155/2012/458368.

Yudong, L., Shihan, W., Yiqian, L., Ning, W., Pinyi, D. and Qiang, Y. (2021) 'The coupled mixing action of the jet mixer and swirl mixer; a novel static micromixer', *Chemical Engineering Research and Design*, Vol. CLXXVII, No. 2022, pp.283–290, DOI: 10.1016/j.cherd.2021.10.040.

Zagorka, B.M., Nabojsa, M.G., Dragoslava, S.D. and Marta, T.R. (2019) 'Application of different k-e turbulence models on combustion process modelling in small-scale pellet stoves for household heating', *Progress in Computational Fluid Dynamics*, Vol. IXX, No. 3, pp.180–191.

Zhang, J.K. (2017) 'Analysis on the effect of Venturi tube structural parameters on fluid flow', *AIP Advances*, pp.1–7, DOI: 10.1063/1.4991441.

Zihzhen, W., Tianyang, L., Fangxiang, W., Lin, G. and Rui, Z. (2020) 'Numerical simulation of polymer dispersion systems for polymer injection on offshore platforms', *ACS Omega*, No. 32, pp.20343–20352.